NANO LETTERS

2007
Vol. 7, No. 6
1631−1636

Hybrid Confocal Raman Fluorescence Microscopy on Single Cells Using Semiconductor Quantum Dots

Henk-Jan van Manen* and Cees Otto

Biophysical Engineering Group, MESA+ Institute for Nanotechnology, and Institute for Biomedical Technology (BMTI), University of Twente, P.O. Box 217, 7500 AE Enschede, The Netherlands

Received March 13, 2007

ABSTRACT

We have overcome the traditional incompatibility of Raman microscopy with fluorescence microscopy by exploiting the optical properties of semiconductor fluorescent quantum dots (QDs). Here we present a hybrid Raman fluorescence spectral imaging approach for single-cell microscopy applications. We show that resonant Raman imaging of flavocytochrome b_{558} at 413.1 nm excitation in QD-labeled neutrophilic granulocytes or nonresonant Raman imaging of proteins and lipids at 647.1 nm excitation in QD-labeled macrophages can be integrated with linear one-photon excitation and nonlinear continuous-wave two-photon excitation fluorescence microscopy of QDs, respectively. The enhanced information content of these two hybrid Raman fluorescence methods provides new multiplexing possibilities for single-cell optical microscopy and intracellular chemical analysis.

Cell and tissue optical microscopies based on label-free vibrational spectroscopy (e.g., infrared,[1−2] spontaneous Raman,[3−4] and nonlinear coherent anti-Stokes Raman scattering[5−6] (CARS) microscopy) have become versatile complementary imaging techniques to fluorescence microscopy because vibrational spectra obtained from small intracellular volumes or tissues display a wealth of molecularly specific information that is usually only obtainable in fluorescence microscopy by labeling the molecules of interest with fluorophores, which may not always be feasible and can introduce perturbations to cell functions. Recent examples of single-cell nonresonant Raman microscopy include the visualization of (i) DNA/RNA, proteins, and lipids in apoptotic HeLa cells,[7] (ii) heme aggregation and denaturation in erythrocytes,[8] (iii) lipid bodies in neutrophilic granulocytes,[9] and (iv) stress-induced changes in lung fibroblasts.[10] We have also employed resonant Raman imaging to selectively visualize changes in the activation and distribution of flavocytochrome b_{558}, the catalytic subunit of the NADPH oxidase enzyme that is critical in the innate immune response,[11] in neutrophilic granulocytes stimulated with soluble or particulate activators.[12−13]

Despite the success of imaging techniques based on vibrational spectroscopy, fluorescence of the sample under investigation has been a drawback of linear spontaneous and resonant Raman spectroscopy. Because the Raman scattering cross-section of cellular constituents is usually orders of magnitude lower than the product of absorption cross-section and quantum yield of common fluorophores, Raman microscopy has traditionally been regarded as incompatible with fluorescence microscopy on fluorophore-labeled or autofluorescent samples. In principle, CARS microscopy is less sensitive to linear intrinsic fluorescence but suffers from a nonresonant background and a low spectral resolution. These drawbacks might severely hamper the identification of subtle changes in the chemical composition of cells, and alleviating them is therefore a topic of considerable recent interest.[5,6,14−19] Although spontaneous Raman microscopy is a relatively slow imaging technique compared to CARS microscopy, it compensates for this disadvantage by the broad bandwidth response. Moreover, the high spectral resolution in spontaneous Raman spectroscopy is not limited by the pulsed nature of the light source, as in CARS. Our aim here is to take full advantage of the richness displayed by vibrational spectra of biological samples by combining rapid fluorescence microscopy of QD-labeled cells with linear resonant or nonresonant Raman microscopy of the same cells. We have previously demonstrated[20] that nonresonant Raman imaging is compatible with continuous-wave two-photon excitation (cw-TPE) fluorescence microscopy of the organic fluorophore Hoechst 33342, which is targeted to the cell nucleus. A large spectral separation is obtained in this case because

* Corresponding author. E-mail: h.w.j.vanmanen@tnw.utwente.nl. Telephone: +31 (0)53 4893466. Fax: +31 (0)53 4891105.

10.1021/nl0705945 CCC: $37.00
Published on Web 05/03/2007

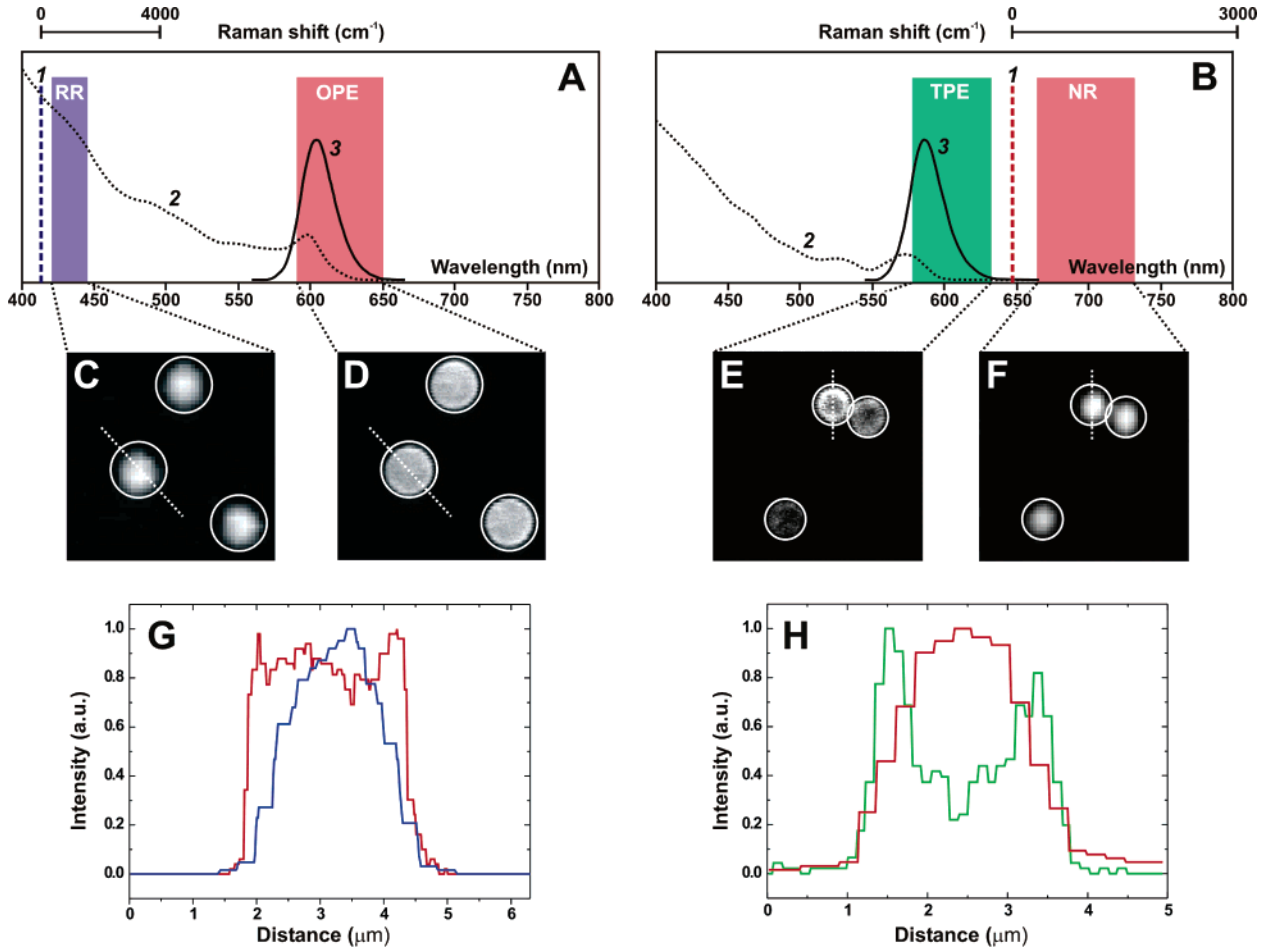

Figure 1. Schematic representation (A,B) and experimental results (C−H) of hybrid Raman-fluorescence microscopy experiments on QD-coated microspheres. (A) RR/OPE strategy using 413.1 nm excitation (dashed vertical line "1"). Spectral windows for detection of RR and OPE fluorescence signals are shown in blue and red, respectively. Absorption ("2") and emission ("3") spectra of Qdot 605 QDs are shown. (B) NR/TPE strategy using 647.1 nm excitation (dashed vertical line "1"). Spectral windows for detection of NR and TPE fluorescence signals are shown in red and green, respectively. Absorption ("2") and emission ("3") spectra of Qdot 585 QDs are shown. (C,D) Raman (C) and OPE fluorescence (D) images of Qdot 605-coated polystyrene microspheres. (E,F) TPE fluorescence (E) and nonresonant Raman (F) images of Qdot 585-coated polystyrene microspheres. Image acquisition details for images C−F are provided in the text. (G,H) Intensity line profiles through the designated microspheres shown in C−F. Line colors correspond to the spectral window colors shown in A,B.

the fluorescence emission occurs at the anti-Stokes side of the laser excitation wavelength, whereas the spontaneous Raman scattering is detected on the Stokes side. TPE fluorescence microscopy can also be combined with CARS microscopy.[21−23]

We anticipated that spectral separation of Raman scattering and one-photon-excitation (OPE) fluorescence emission, both on the Stokes side of the excitation wavelength, might be possible using fluorophores with a very large Stokes shift. Semiconductor quantum dot (QD) nanocrystals, which are under intense investigation because of their excellent fluorescence properties in, e.g., in vitro live-cell microscopy and in vivo imaging of whole organisms,[24−27] display such a required Stokes shift. Moreover, they possess a large absorption cross-section and a narrow emission bandwidth (∼20−40 nm, fwhm) compared to conventional, small-molecule fluorophores. Here, we show that resonant Raman spectroscopy and imaging on single cells can be combined with OPE fluorescence microscopy by incubation of cells with nanosized quantum dots. Moreover, we demonstrate that cw-TPE microscopy on QD-labeled cells is fully compatible with single-cell nonresonant Raman microscopy, similar to our previously reported results.[20] A clear advantage of using QDs is that they can be targeted to selective organelles or proteins in a cell by conjugating them to ligands, antibodies, or peptide localization sequences and performing well-established cellular labeling protocols.[24−28] The QD fluorescence emission may then be correlated to the Raman scattering signal from endogenous biomolecules, providing information that is difficult or impossible to obtain using either method alone. Another versatile hybrid microscopy strategy involving QDs is combined electron microscopy (EM) and fluorescence microscopy on cell and tissue sections.[29,30] However, in contrast to the combined Raman/fluorescence strategy reported here, combined EM/fluorescence cannot be performed on living cells.

Our two spectral strategies for combining single-cell confocal Raman and fluorescence microscopy on a single optical setup are schematically outlined in Figure 1. At 413.1 nm excitation, the resonant Raman (RR) signal from cells at 420−445 nm (∼400−1750 cm^{-1}) is combined with one-photon-excitation (OPE) fluorescence emission of QDs (Qdot

605 streptavidin conjugate[31]) detected at 590−650 nm, as shown in Figure 1A. In this strategy termed RR/OPE, both the RR signal and the QD fluorescence are detected on the Stokes side of the excitation.

Alternatively, the strategy termed NR/TPE shown in Figure 1B combines the two-photon excitation fluorescence emission of QDs (Qdot 585 streptavidin conjugate[31]) at the anti-Stokes side of the 647.1 nm excitation with the Stokes nonresonant Raman (NR) signal from cells at 660−730 nm (∼300−1800 cm^{-1}, fingerprint region) or 770−870 nm (∼2500−4000 cm^{-1}, high-frequency region). Hybrid confocal Raman and fluorescence microscopy experiments were performed as reported before[20] by point-scanning the excitation beam over the sample and placing a foldable mirror in the optical detection path to switch between Raman spectroscopy, using a spectrograph-CCD camera combination, and fluorescence detection, using an avalanche photodiode (APD) point detector (see Supporting Information Figure S2).

As a model system to test the feasibility of the RR/OPE and NR/TPE strategies for combining Raman and fluorescence microscopy experiments, we used nonfluorescent biotinylated polystyrene (PS) microspheres (diameter 2.2 μm) that were uniformly coated (see Supporting Information) with streptavidin-conjugated Qdots 605 (RR/OPE) or Qdots 585 (NR/TPE). The results of representative hybrid confocal fluorescence and Raman microscopy experiments on these microspheres are shown in Figure 1C−F. The RR/OPE experiment was performed by first recording a fluorescence image (Figure 1D) using 5 μW of 413.1 nm excitation power, 128 × 128 pixels and an accumulation time of 0.25 ms per pixel (total imaging time 4.1 s). Subsequently, a Raman image (Figure 1C, reconstructed in the strong 1000 cm^{-1} Raman band of polystyrene) with 1 mW excitation power, 32 × 32 pixels, and 1 s accumulation time per pixel was recorded (total exposure time 17 min). Comparison between the fluorescence and the Raman image shows that the microspheres appear slightly larger in the fluorescence image due to diffraction effects of the QD rim around the PS microspheres, adding approximately 0.5 μm to the microsphere diameter. This is clearly reflected by the intensity line profiles through a microsphere, as plotted in Figure 1G. Fluorescence intensity maxima can be seen at the steep edges of the microsphere, which exemplify the lateral resolution of the imaging system (red line in Figure 1G). Because of the 2.8 μm axial resolution (fwhm) of our confocal setup at this wavelength, calculated using a Gaussian beam approximation,[32] these maxima are not very pronounced. Nevertheless, the absence of edge maxima in the Raman intensity profile (blue line in Figure 1G) demonstrates that no spectral overlap occurs between the polystyrene Raman signal and the fluorescence emission of QDs. The NR/TPE experiment was performed by recording a TPE fluorescence image (Figure 1E) using 100 mW of cw 647.1 nm excitation power, a 577.5−632.5 nm bandpass emission filter, 128 × 128 pixels, and an accumulation time of 1 ms per pixel (total imaging time 16.4 s), followed by a Raman image (Figure 1F, reconstructed in the strong 1000 cm^{-1} Raman band of polystyrene) with 100 mW excitation power, 32 × 32 pixels and 0.5 s accumulation time per pixel (total exposure time 8.5 min). The TPE fluorescence intensity profile (Figure 1H, green line) shows more pronounced edge maxima than the OPE intensity profile (Figure 1G, red line), which implies a better axial resolution in the TPE than in the OPE fluorescence experiment, as expected for nonlinear excitation. The "slow" intensity increase in the Raman line profiles in parts G and H of Figure 1 reflects the shape of the microspheres convoluted with the point-spread function of the imaging system because the 2.2 μm diameter PS beads are spheres on the scale of the diffraction limit at 413.1 and 647.1 nm excitation.

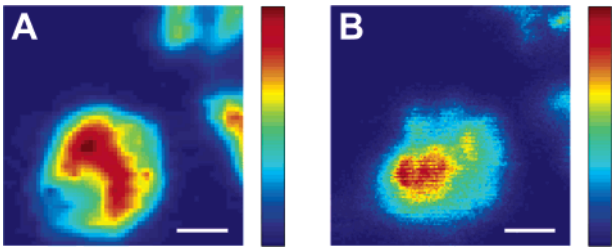

Figure 2. Combined RR/OPE microscopy on Qdot 605-labeled neutrophils at 413.1 nm excitation. (A) RR spectral image constructed from the 1360-cm^{-1} band of reduced flavocytochrome b_{558}. (B) OPE fluorescence image of QDs detected at 590−650 nm. Excitation powers and pixel acquisition times were 1 mW/1 s and 50 μW/0.25 ms for the RR and OPE fluorescence experiment, respectively. The Raman and fluorescence intensities in A and B scale from 0 to 370 and from 0 to 300 counts, respectively. Scale bar, 3 μm.

For combined RR/OPE experiments on QD-labeled cells, we used neutrophilic granulocytes. We have performed extensive RR spectroscopy and microscopy experiments to characterize and visualize flavocytochrome b_{558} that is abundantly present in these cells..[12,13,33−36] Flavocytochrome b_{558} converts oxygen to superoxide (O_2^-) upon activation of neutrophils, which is subsequently converted to an array of reactive oxygen species that is used by these leukocytes to destroy phagocytosed microorganisms.[11] We first established that, under the conditions used for RR imaging on neutrophils, the contribution of the QD fluorescence signal to the Raman spectral window (∼400−1750 cm^{-1}, 420−445 nm) is very low. Exposure of a 100 nM Qdot 605 solution in PBS to 1 mW of 413.1 nm excitation led to a rather constant increase of 1−2 counts (average 1.4) per channel in the 400−1750 cm^{-1} region on the CCD chip (1 s accumulation time). For comparison, we typically measure ∼45 counts (maximum pixel intensity, not integrated intensity) under the same conditions for the strongest RR band of intracellular flavocytochrome b_{558}. Thus, the OPE fluorescence emission of QDs measured under RR conditions leads to a slight increase in background in the 400−1750 cm^{-1} region. This does not prevent in any way the acquisition and identification of the RR signals of flavocytochrome b_{558} from neutrophilic granulocytes (vide infra).

We next incubated neutrophils for 30 min with 20 nM streptavidin-conjugated Qdots 605, fixed the cells, and performed combined OPE fluorescence and RR microscopy experiments (in that order). The images shown in Figure 2

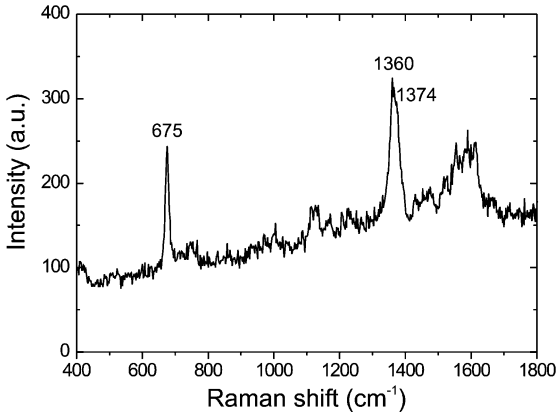

Figure 3. Average RR spectrum from a live QD-labeled neutrophil. Strong marker bands for flavocytochrome b_{558} are indicated. Excitation power 1 mW, accumulation time 10 s.

reveal a rather homogeneous distribution of both flavocytochrome b_{558} (Figure 2A) and the QDs (Figure 2B) in the imaged neutrophil.

The RR image was constructed in the 1360 cm^{-1} band of reduced[37] flavocytochrome b_{558} (a typical RR spectrum from a QD-labeled neutrophil is shown in Figure 3).

We found that OPE fluorescence microscopy on neutrophils using QDs can also be combined with live-cell RR microspectroscopy. After fluorescence imaging of living neutrophils incubated with QDs, we recorded average RR spectra from the same cells by fast scanning over them for 10 s while acquiring the RR signal (Figure 3). The resulting RR spectra are very similar to previously reported RR spectra from live unlabeled neutrophils,[33−36] which demonstrates that labeling neutrophils with QDs does not affect RR spectra recorded from these cells. This versatile combination therefore allows one to quickly scan a cell by fluorescence microscopy (revealing intracellular QDs targeted to specific sites, for example) and subsequently zoom in on regions of interest and perform intracellular chemical analysis by RR microspectroscopy.

Although QDs are widely considered as very stable fluorophores, we noticed that they are prone to photobleaching at high-power 413.1 nm excitation. After RR imaging experiments on neutrophils, performed at 1 mW excitation power (corresponding to 1.3 MW/cm^2), the QD fluorescence of the imaged cells had disappeared. We therefore employed fluorescence microscopy before RR microscopy. In contrast, fluorescence microscopy in combination with RR microspectroscopy (by fast scanning over the cell) did not lead to photobleaching because fluorescence images (recorded at 5 μW excitation power) before and after the acquisition of a RR spectrum (at 1 mW) were very similar. This suggests that the illumination dose rather than the excitation power poses limits on the time that QDs are fluorescent. Bleaching of single QDs in air at 468 nm excitation (20 kW/cm^2), as reported by Van Sark et al.,[38] has been ascribed to photoinduced oxidation, as suggested by the observation of a faster fading of luminescence in air compared to nitrogen.

Before combined NR/TPE experiments on QD-labeled cells were undertaken, we investigated the possibility for

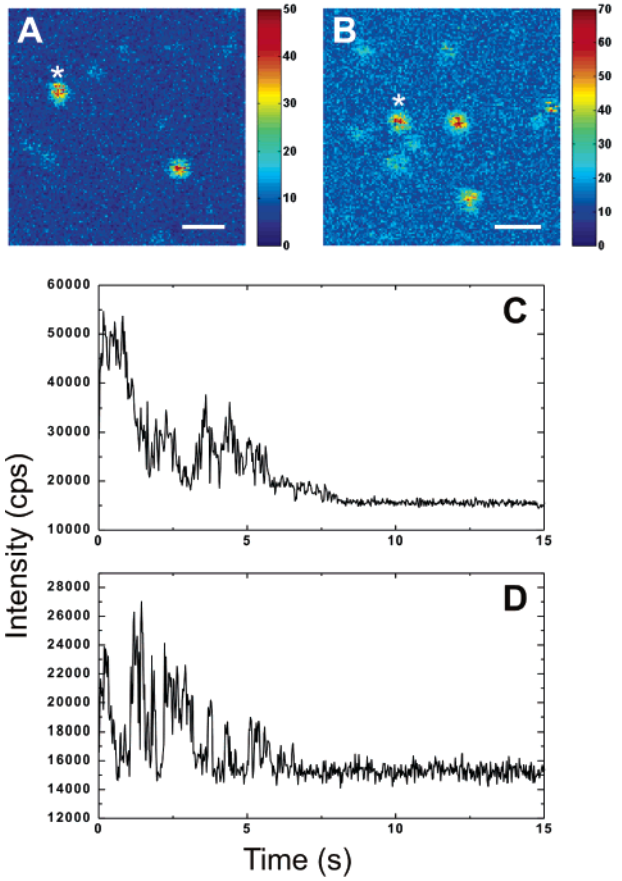

Figure 4. (A,B) cw-TPE fluorescence images of streptavidin-conjugated Qdots 585 in a PVA matrix spin-coated onto a glass cover slip. Excitation 647.1 nm (170 mW), detection at 577.5−632.5 nm. Image A: 128 × 128 pixels, 1 ms/pixel. Image B: 128 × 128 pixels, 2.5 ms/pixel. (C,D) Fluorescence intensity time traces (25 ms bin) recorded at the spots marked with asterisks in A and B, respectively. Scale bars in A and B represent 1 μm.

detecting single QDs using cw-TPE fluorescence because it is of interest to establish a detection limit for QDs in cellular applications of combined NR/TPE microscopy (vide infra). Reports on cw-TPE fluorescence microscopy of biological specimens have so far focused on chromosomes and cells containing high local concentrations of DNA-labeling dyes such as DAPI and Hoechst 33342.[39−41] However, a low-temperature (1.2 K) cw-TPE fluorescence microscopy study at 810 nm excitation demonstrated the detection of single CdS nanocrystallites in a poly(vinyl alcohol) (PVA) matrix.[42] We spin-coated a 0.25 nM solution of streptavidin-conjugated Qdots 585 in 2% PVA onto a glass cover slip and performed cw-TPE fluorescence microscopy at room temperature. The images in parts A and B of Figure 4 reveal spots of ∼400 nm diameter, which is in agreement with the $1/e^2$ beam waist diameter calculated from a Gaussian beam approximation (349 nm).[20] Parts C and D of Figure 4 show fluorescence intensity time traces from the spots marked with asterisks in parts A and B of Figure 4, respectively. Discrete on/off fluorescence blinking is a characteristic property of single QDs,[43−46] although it has recently been reported that a continuous emission state distribution model is more appropriate in describing the observed fluorescence dynamics of single QDs.[47] Nevertheless, the observed intermittency

in the traces shown in Figure 4C and D confirms that individual QDs can be detected using cw-TPE fluorescence microscopy under ambient conditions.

We next combined nonresonant Raman imaging of proteins and lipids with cw-TPE fluorescence microscopy on QD-labeled murine RAW 264.7 macrophages. Macrophages were incubated for 2 h with 20 nM streptavidin-conjugated Qdots 585, fixed with paraformaldehyde, and imaged by cw-TPE fluorescence and NR microscopy experiments (in that order). In contrast to our previous studies showing that NR imaging can be performed at a 647.1 nm excitation dose of 100 mJ per image pixel without affecting the Raman spectra or cell morphology,[7,9] we found that the use of such high doses on QD-labeled macrophages led to the disruption of cell integrity, as judged from transmitted light microscopy, and to a ~10−30 fold increase in the background of Raman spectra from certain cellular locations, thereby overwhelming the Raman signal in these regions. We speculate that, at too-high excitation doses of 647.1 nm laser light, localized heating occurs due to the excessive absorption of energy by QDs. This might lead to photothermal cell ablation, a process that also occurs in near-infrared-illuminated cells incubated with gold nanoshells[48,49] or gold nanorods[50] and is used intentionally with these nanoparticles to destroy tumor cells. We could avoid ablation, which is undesired during imaging, by using excitation doses of 25 mJ and 6.25 μJ per image pixel for NR and cw-TPE fluorescence microscopy, respectively. NR images were constructed by integrating the Raman signal in the 2800−3050 cm^{-1} high-frequency region, which has strong contributions from aliphatic C−H stretching vibrational modes that are mostly present in proteins and lipids. Figure 5A shows a nonresonant Raman image of the protein and lipid distribution in a QD-labeled macrophage.

The average NR spectrum from the cell, which contains bands at ~2850 (symmetric CH_2 stretch), ~2890 (asymmetric CH_2 stretch), and 2935 cm^{-1} (CH stretch), is shown in Figure 5C. The corresponding TPE fluorescence image of the same cell, shown in Figure 5B, reveals that the QDs are mostly present in intracellular vesicles. The accumulation of QDs in vesicles was observed in all recorded TPE fluorescence images of QD-labeled macrophages and is caused by nonspecific internalization via endo-, pino-, and/or phagocytosis mechanisms, as amply described in the literature.[51−54] Occasionally, a vesicular staining pattern was also observed in OPE fluorescence images of QD-labeled neutrophils, in contrast to the diffuse QD distribution shown in Figure 2B. Similar to the RR/OPE strategy, we found no cross-talk between the nonresonant Raman signal from macrophages and the fluorescence emission from QDs. This indicates that the NR and cw-TPE fluorescence signals are spectrally well-separated, as schematically depicted in Figure 1B.

In conclusion, we have exploited the optical properties of nanosized QDs to develop two new strategies for combining confocal Raman microscopy with confocal fluorescence microscopy on QD-labeled biological cells. First, we have shown that resonant Raman microspectroscopy and imaging of flavocytochrome b_{558} in neutrophilic granulocytes at 413.1 nm excitation is fully compatible with linear fluorescence microscopy of intracellular QDs. Second, the continuous-wave two-photon-excited fluorescence of QDs in macrophages does not interfere with the nonresonant Raman signals of proteins and lipids from these cells. As these hybrid Raman fluorescence strategies should be applicable to any cell type that is amenable to labeling with QDs and should also be suitable for other excitation wavelengths that can be used to excite QDs (e.g., the commonly used 488 or 514 nm lines from Ar^+ gas lasers), we envision that hybrid Raman fluorescence microscopy will offer new prospects for integrating QD imaging on cells with spatially resolved, detailed intracellular chemical analysis by broadband Raman microspectroscopy.

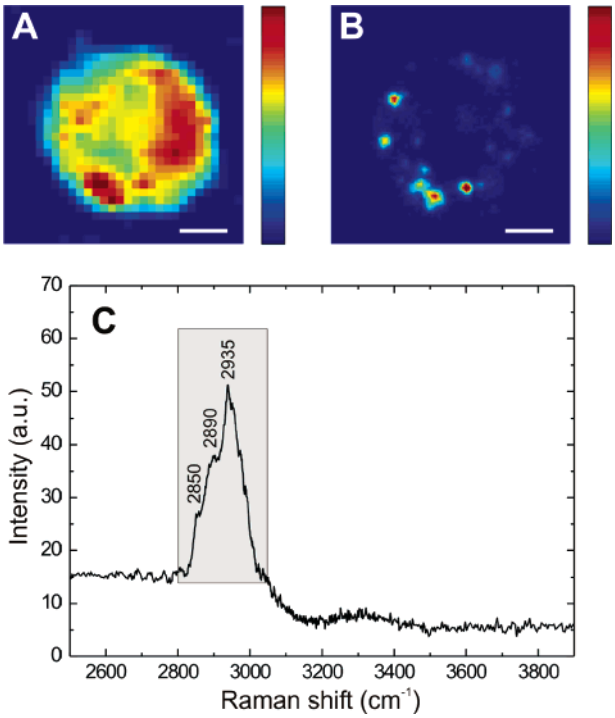

Figure 5. Combined NR/TPE microscopy on Qdot 585-labeled macrophages at 647.1 nm excitation. (A) NR spectral image constructed from the high-frequency region (2800−3050 cm^{-1}) of proteins and lipids. (B) TPE fluorescence image of QDs detected at 577.5−632.5 nm. Excitation powers and pixel acquisition times were 25 mW/1 s and 25 mW/0.25 ms for the NR and TPE fluorescence experiments, respectively. (C) Difference NR spectrum obtained by subtracting the buffer spectrum from the average NR spectrum of the cell shown in A. The major contribution to the indicated spectral region (gray box) is from aliphatic C−H stretching vibrational modes. The Raman and fluorescence intensities in A and B scale from 0 to 5000 and from 0 to 50 counts, respectively. Scale bars in A and B represent 3 μm.

Acknowledgment. Financial support from the Landsteiner Foundation for Blood Transfusion Research (Amsterdam, The Netherlands) and the $MESA^+$ Institute for Nanotechnology (University of Twente) is gratefully acknowledged.

Supporting Information Available: Materials and Methods and Supporting Figures. This material is available free of charge via the Internet at http://pubs.acs.org.

References

(1) Wetzel, D. L.; LeVine, S. M. *Science* **1999**, *285*, 1224−1225.
(2) Levin, I. W.; Bhargava, R. *Annu. Rev. Phys. Chem.* **2005**, *56*, 429−474.
(3) Notingher, I.; Hench, L. L. *Expert Rev. Med. Devices* **2006**, *3*, 215−234.
(4) Navratil, M.; Mabbott, G. A.; Arriaga, E. A. *Anal. Chem.* **2006**, *78*, 4005−4020.
(5) Cheng, J.-X.; Xie, X. S. *J. Phys. Chem. B* **2004**, *108*, 827−840.
(6) Rodriguez, L. G.; Lockett, S. J.; Holtom, G. R. *Cytometry A* **2006**, 779−791.
(7) Uzunbajakava, N.; Lenferink, A.; Kraan, Y.; Volokhina, E.; Vrensen, G.; Greve, J.; Otto, C. *Biophys. J.* **2003**, *84*, 3968−3981.
(8) Wood, B. R.; Hammer, L.; Davis, L.; McNaughton, D. *J. Biomed. Opt.* **2005**, *10*, 014005.
(9) Van Manen, H.-J.; Kraan, Y. M.; Roos, D.; Otto, C. *Proc. Natl. Acad. Sci. U.S.A.* **2005**, *102*, 10159−10164.
(10) Krafft, C.; Knetschke, T.; Funk, R. H.; Salzer, R. *Anal. Chem.* **2006**, *78*, 4424−4429.
(11) Cross, A. R.; Segal, A. W. *Biochim. Biophys. Acta* **2004**, *1657*, 1−22.
(12) Van Manen, H.-J.; Uzunbajakava, N.; Van Bruggen, R.; Roos, D.; Otto, C. *J. Am. Chem. Soc.* **2003**, *125*, 12112−12113.
(13) Van Manen, H.-J.; Kraan, Y. M.; Roos, D.; Otto, C. *J. Phys. Chem. B* **2004**, *108*, 18762−18771.
(14) Volkmer, A. *J. Phys. D: Appl. Phys.* **2005**, *38*, R59−R81.
(15) Potma, E. O.; Evans, C. L.; Xie, X. S. *Opt. Lett.* **2006**, *31*, 241−243.
(16) Ganikhanov, F.; Evans, C. L.; Saar, B. G.; Xie, X. S. *Opt. Lett.* **2006**, *31*, 1872−1874.
(17) Burkacky, O.; Zumbusch, A.; Brackmann, C.; Enejder, A. *Opt. Lett.* **2006**, *31*, 3656−3658.
(18) Kee, T. W.; Zhao, H.; Cicerone, M. T. *Opt. Express* **2006**, *14*, 3631−3640.
(19) Jurna, M.; Korterik, J. P.; Offerhaus, H. L.; Otto, C. *Appl. Phys. Lett.* **2006**, *89*, 251116.
(20) Uzunbajakava, N.; Otto, C. *Opt. Lett.* **2003**, *28*, 2073−2075.
(21) Wang, H.; Fu, Y.; Zickmund, P.; Shi, R.; Cheng, J.-X. *Biophys. J.* **2005**, *89*, 581−591.
(22) Evans, C. L.; Potma, E. O.; Puoris'Haag, M.; Côté, D.; Lin, C. P.; Xie, X. S. *Proc. Natl. Acad. Sci. U.S.A.* **2005**, *102*, 16807−16812.
(23) Nan, X.; Potma, E. O.; Xie, X. S. *Biophys. J.* **2006**, *91*, 728−735.
(24) Michalet, X.; Pinaud, F. F.; Bentolila, L. A.; Tsay, J. M.; Doose, S.; Li, J. J.; Sundaresan, G.; Wu, A. M.; Gambhir, S. S.; Weiss, S. *Science* **2005**, *307*, 538−544.
(25) Medintz, I. L.; Uyeda, H. T.; Goldman, E. R.; Mattoussi, H. *Nat. Mater.* **2005**, *4*, 435−446.
(26) Alivisatos, A. P.; Gu, W.; Larabell, C. *Annu. Rev. Biomed. Eng.* **2005**, *7*, 55−76.
(27) Gao, X.; Yang, L.; Petros, J. A.; Marshall, F. F.; Simons, J. W.; Nie, S. *Curr. Opin. Biotechnol.* **2005**, *16*, 63−72.
(28) Derfus, A. M.; Chan, W. C. W.; Bhatia, S. N. *Adv. Mater.* **2004**, *16*, 961−966.
(29) Nisman, R.; Dellaire, G.; Ren, Y.; Li, R.; Bazett-Jones, D. P. *J. Histochem. Cytochem.* **2004**, *52*, 13−16.
(30) Giepmans, B. N. G.; Deerinck, T. J.; Smarr, B. L.; Jones, Y. Z.; Ellisman, M. H. *Nat. Methods* **2005**, *2*, 743−749.
(31) From Quantum Dot Corporation, now Invitrogen.
(32) De Grauw, C. J.; Sijtsema, N. M.; Otto, C.; Greve, J. *J. Microsc.* **1997**, *188*, 273−279.
(33) Sijtsema, N. M.; Otto, C.; Segers-Nolten, G. M. J.; Verhoeven, A. J.; Greve, J. *Biophys. J.* **1998**, *74*, 3250−3255.
(34) Otto, C.; Sijtsema, N. M.; Greve, J. *Eur. Biophys. J.* **1998**, *27*, 582−589.
(35) Sijtsema, N. M.; Tibbe, A. G. J.; Segers-Nolten, I. G. M. J.; Verhoeven, A. J.; Weening, R. S.; Greve, J.; Otto, C. *Biophys. J.* **2000**, *78*, 2606−2613.
(36) Van Manen, H.-J.; Van Bruggen, R.; Roos, D.; Otto, C. *Antioxid. Redox Signaling* **2006**, *8*, 1509−1522.
(37) We reduced the flavocytochrome b_{558} molecules by adding a few grains of sodium dithionite in order to reduce photobleaching of the flavocytochrome b_{558} RR signal (see also ref 13).
(38) Van Sark, W. G. J. H. M.; Frederix, P. L. T. M.; Bol, A. A.; Gerritsen, H. C.; Meijerink, A. *ChemPhysChem* **2002**, *3*, 871−879.
(39) Booth, M. J.; Hell, S. W. *J. Microsc.* **1998**, *190*, 298−304.
(40) Hell, S. W.; Booth, M.; Wilms, S.; Schnetter, C. M.; Kirsch, A. K.; Arndt-Jovin, D. J.; Jovin, T. M. *Opt. Lett.* **1998**, *23*, 1238−1240.
(41) Kirsch, A. K.; Subramaniam, V.; Striker, G.; Schnetter, C.; Arndt-Jovin, D. J.; Jovin, T. M. *Biophys. J.* **1998**, *75*, 1513−1521.
(42) Van Oijen, A. M.; Verberk, R.; Durand, Y.; Schmidt, J.; Van Lingen, J. N. J.; Bol, A. A.; Meijerink, A. *Appl. Phys. Lett.* **2001**, *79*, 830−832.
(43) Nirmal, M.; Dabbousi, B. O.; Bawendi, M. G.; Macklin, J. J.; Trautman, J. K.; Harris, T. D.; Brus, L. E. *Nature* **1996**, *383*, 802−804.
(44) Neuhauser, R. G.; Shimizu, K. T.; Woo, W. K.; Empedocles, S. A.; Bawendi, M. G. *Phys. Rev. Lett.* **2000**, *85*, 3301−3304.
(45) Hohng, S.; Ha, T. *J. Am. Chem. Soc.* **2004**, *126*, 1324−1325.
(46) Yao, J.; Larson, D. R.; Vishwasrao, H. D.; Zipfel, W. R.; Webb, W. W. *Proc. Natl. Acad. Sci. U.S.A.* **2005**, *102*, 14284−14289.
(47) Zhang, K.; Chang, H.; Fu, A.; Alivisatos, A. P.; Yang, H. *Nano Lett.* **2006**, *6*, 843−847.
(48) Hirsch, L. R.; Stafford, R. J.; Bankson, J. A.; Sershen, S. R.; Rivera, B.; Price, R. E.; Hazle, J. D.; Halas, N. J.; West, J. L. *Proc. Natl. Acad. Sci. U.S.A.* **2003**, *100*, 13549−13554.
(49) Loo, C.; Lowery, A.; Halas, N.; West, J.; Drezek, R. *Nano Lett.* **2005**, *5*, 709−711.
(50) Huff, T. B.; Tong, L.; Zhao, Y.; Hansen, M. N.; Cheng, J.-X.; Wei, A. *Nanomedicine* **2007**, *2*, 125−132.
(51) Parak, W. J.; Boudreau, R.; Le, Gros, M.; Gerion, D.; Zanchet, D.; Micheel, C. M.; Williams, S. C.; Alivisatos, A. P.; Larabell, C. *Adv. Mater.* **2002**, *14*, 882−885.
(52) Hanaki, K.; Momo, A.; Oku, T.; Komoto, A.; Maenosono, S.; Yamaguchi, Y.; Yamamoto, K. *Biochem. Biophys. Res. Commun.* **2003**, *302*, 496−501.
(53) Jaiswal, J. K.; Mattoussi, H.; Mauro, J. M.; Sanford, S. M. *Nat. Biotechnol.* **2003**, *21*, 47−51.
(54) Parak, W. J.; Pellegrino, T.; Plank, C. *Nanotechnology* **2005**, *16*, R9−R25.

NL0705945